AUTOMATIC INCORPORATION OF RIVERBANK FAILURES IN TWO-DIMENSIONAL FLOOD MODELING

Ouchebri, Ismail[1]; Mahdi, Tew-Fik[2]

[1] Ph.D Student, Département des génies Civil, Géologique et des Mines (CGM), École Polytechnique de Montréal, C.P. 6079, succursale Centre-Ville, Montréal, QC H3C 3A7, Canada. Email: ismail.ouchebri@polymtl.ca

[2] Professor, Département des génies Civil, Géologique et des Mines (CGM), École Polytechnique de Montréal, C.P. 6079, succursale Centre-Ville, Montréal, QC H3C 3A7, Canada (Corresponding author). Email: tewfik.mahdi@polymtl.ca

Abstract

Riverbanks undergo changes caused not only by river hydraulics, mainly sediment erosion and deposition processes, but also by the possible landslides that eventually change the channel bank profiles. Those failures are an important form of alluvial channel adjustments but are usually difficult to include during morphodynamic modeling. This paper proposes a novel approach combining a 2D depth-averaged hydrodynamic, sediment transport and mobile-bed model, SRH-2D, a limit equilibrium slope-stability model, BISHOP, and a bank failure sediment redistribution submodel, REDISSED, into a fully automatic and continuous dynamic simulation to predict vertical bed and lateral bank changes for a river reach undergoing exceptional flooding. The in-stream vertical fluvial changes predicted with the SRH-2D model will be automatically used to update the riverbank geometry profile by profile and assess their geotechnical stability to rotational slip failures with a developed slope-stability model based on Bishop's simplified method. A cone-shaped sliding area is defined in case the driving forces exceed the stabilizing forces. All mesh nodes located within the mass wasting zone will be automatically updated, allowing a new bank face form. The failed materials will be redistributed in the transect according to the geometry of the landslides observed at the study site. The Outaouais River at Notre-Dame-Du Nord, Quebec, is used to test the coupling procedure. Up to 100 m of bank retreat was predicted, and more than 20 cross-

sections were reshaped. Typical results showing the effectiveness of the developed framework are presented and discussed.

Author keywords: Streambank erosion; Riverbank failure; Two-dimensional modeling; SRH-2D; BISHOP; Automatic coupling; Sediment redistribution.

Introduction

Rivers are dynamic systems governed by hydraulic and sediment transport processes. Over time, meandering channels respond to changing conditions in the environment by modifying their cross-sectional and planform shapes. In fact, alluvial rivers in nature display morphological adjustments in response to the exerted stresses, especially erosion, triggered by the interaction of flow and the riverbed or banks. Streambank erosion is considered one of the most important processes in adjusting alluvial systems (Langendoen et al. 2009). It is a natural process that occurs when the forces exerted by flowing water exceed the resisting forces of the bank materials and vegetation (Simon et al. 2000). This type of erosion is generally regarded as a combination of the fluvial entrainment of bank materials by flowing water and the mass failure of unstable banks (ASCE Task Committee on Hydraulics 1998; Darby et al. 2007; Langendoen and Simon 2008). From a numerical perspective, riverbank failures are often overlooked when modeling channel morphological evolution; the multidimensional hydrodynamic and bed evolution models only evaluate fluvial erosion and need to be coupled with bank erosion submodels to assess channel morphological adjustments evoked by riverbank geotechnical mass failures.

To properly examine river morphological evolution, researchers and practitioners have established a large number of assumptions, developed tools and models and utilized different approaches and techniques to combine both fluvial erosion and mass wasting (Lai et al. 2012; Lai et al. 2015; Langendoen et al. 2016; Langendoen and Simon 2008; Mahdi and Marche 2003; Rousseau et al. 2017). Notwithstanding the various employed strategies, they all aim to integrate the different physical processes responsible for bank retreat into one runnable solution by coupling physical and process-based models. One of those solutions consisted of combining the flowing-water and bank erosion computer models with mass failure predictive models. (Mahdi and Marche 2003) were probably the first to simulate the morphologic adjustment of both the bed and the banks over a long river reach (9.8 km) in a natural meandering river

system by coupling one-dimensional (1D) erosion and sediment transport model GSTARS-1D (Yang et al. 1998) with a bank-stability model called BISHOP to assess the circular failures of nonhomogenous cohesive banks (Mahdi and Merabtene 2010; Mahdi and Marche 2003); the combined model was later used to evaluate bank retreat of the river downstream of the Première Chute Dam (Mahdi 2004) in Quebec and yielded a promising results. However, the mobile-bed model GSTARS-1D (Yang et al. 1998) uses a simple theory in that the channel geometry adjustments can be vertical or lateral depending on the minimum unit stream power theory (Yang 1976), an approach that can be used only for short- and medium-term predictions (Simon et al. 2007). Similarly, (Langendoen and Simon 2008) merged an unsteady one-dimensional channel evolution and physically based model called CONCEPTS (Langendoen 2000) with a geotechnical submodel to simulate the streambank planar failures of riverbanks over the bendway of Goodwin Creek, Mississippi, and later over two incised streams in northern Mississippi, James Creek and the Yalobusha River (Langendoen et al. 2009). (Motta et al. 2012) coupled the physically based algorithms of the channel evolution model CONCEPTS (Langendoen 2000) with the (2D) hydrodynamic and migration RVR Meander model (Abad and Garcia 2006) to simulate meander migration at the reach scale. Recently, (Motta et al. 2012) simulated bank retreat also using the one-dimensional computer model CONCEPTS (Langendoen 2000) to investigate the impact of the variability of erodibility parameters on the model's lateral retreat predictions. However, CONCEPTS (Langendoen 2000) and likely GSTARS-1D (Yang et al. 1998) are 1D models they do not incorporate corrections for secondary currents and transversal bed slope, and hydraulics are not adequately resolved to predict bank erosion. Therefore, their applicability to meander bends might underestimate the shear stress along the streambank. Indeed, the increased shear stresses for the CONCEPTS (Langendoen 2000) model are represented by a reduction in resistance to erosion of the bank material (Langendoen and Simon 2008); the model is unable to predict the increased hydraulic forces acting on the outer banks caused by the helical flow patterns in the bends, which limits its applicability to only in regions where the phenomena can be neglected (Lai et al. 2012). Moreover, (Abad and Garcia 2006) showed less variation in predicted retreat by the one-dimensional model compared to the incorporated erodibility parameters derived from streambank tests and, more importantly, stressed the need for two- or three-dimensional modeling.

The coupling between riverbank mass failure algorithms and one-dimensional computer models was probably the only way to account for streambank erosion as an important process of river morphological adjustment, despite the simplified physically based equations implemented and the relevant assumptions involved. In recent years, researchers have taken advantage of two-dimensional (2D) morphodynamic numerical models to better understand the interactions between fluvial erosion and mass wasting. (Rinaldi et al. 2008) enhanced our comprehension of this matter by coupling the different components of bank retreat separately using the 2D depth-averaged hydrodynamic model (Deltares Delft 3D) with the commercial groundwater model (GeoSlope, SEEP/W) and the bank stability analysis model (GeoSlope, SLOPE/W) and applied it in a reach-scale hydraulics study within the river bend of the Cecina River, Italy. Despite the overall success of highlighting the roles of fluvial erosion and mass failure driven by hydrodynamic conditions and geotechnical factors, the (Rinaldi et al. 2008) approach loosely accounted for feedbacks between the eroded bank and the flow and simply ignored bed-level changes. In addition, the approach is computationally expensive in terms of the time needed for manual remeshing, making it strictly convenient to simulate a single flood event. Recently, (Rousseau et al. 2017) developed and coupled a riparian vegetation module and a geotechnical algorithm with the two-dimensional solver Telemac-Mascaret (Galland et al. 1991) to predict bank retreat for a semialluvial meandering reach (Medway Creek, Ontario, Canada). The study addressed the effects of plants on the mechanical properties of riverbanks and evaluated the geotechnical stability of the banks independently of the hydrodynamic mesh. It is among the rarest studies to include mass wasting and vegetation processes over a long spatiotemporal scale. (Lai et al. 2015) coupled the deterministic bank stability and toe erosion model (BSTEM) (Simon et al. 2011) developed by the National Sedimentation Laboratory to the 2D depth-averaged hydraulic and sediment transport model SHR-2D (Lai 2010) to predict streambank retreat and planform development. (Lai et al. 2015) evaluated the bank erosion using the near-bank bed shear stress computed by SRH-2D (Lai 2010) and manually moved the mesh to account for the bank toe displacement, an approach that might be very costly in terms of time needed to readjust the mesh and especially, as the researchers acknowledged, the time required to update and interpolate variables. Later, (Lai 2017) extended the previous moving mesh approach to the fixed mesh method and showed that it is often useful to combine both approaches to improve the robustness of the numerical model and thus

accurately predict vertical stream bed changes and lateral streambank erosion for complex systems. In both cases, bank geometries and their erosion are treated separately from SRH-2D (Lai 2010) components. A strategy that allows adequate representation of the bank geometry is often difficult using two-dimensional models that generally reduce bank profiles to a single linear segment.

The state-of-the-art described above presents the most recent studies coupling multiple versions of one-dimensional or two-dimensional models simulating both bed and bank adjustments. Most of those studies are time consuming if applied on a long-reach scale. Moreover, to correctly represent bank geometry within two-dimensional mobile-bed models, geotechnical evaluations are performed independently from the mesh. Thus, in the case of bank retreat, the mesh needs to be readjusted manually, which makes the coupling procedure strictly practical on a limited-size channel. Furthermore, since there is no consensus among researchers considering the redistribution of the derived bank materials, morphodynamical studies simply omit or utilize *ad hoc* approaches to redeposit the failed blocks (Darby and Delbono 2002; Nagata et al. 2000; Pizzuto 1990). In this article, the authors aim to overcome these difficulties by developing a new platform capable of the following: first, describing adequately the stratigraphy and bank geometry of the cross-sections, along which slope-stability assessments are performed, in a 2D mesh without necessarily needing to idealize them; second, assessing their geotechnical stability to rotational failures using an automatic search routine capable of identifying the minimum factor of safety at the potentially unstable riverbanks; third, and most importantly, redistributing slump blocks onto the 2D mesh based on the topographic form of the failed materials in the study area while conserving the mass; and fourth, simulating the feedbacks between the coupled models at each time step automatically, including the mesh movement, without user intervention. The developed procedure is an easy-to-use and time-saving tool for evaluating streambank retreat due to both fluvial erosion and geotechnical failure in long-reach scale modeling systems. Details of the pairing scheme are described in the following sections. The model is applied to the analysis of the evolution of a river reach several kilometers downstream of a dam break scenario.

Overview of the model components

In the present modeling investigation, we combine the 2D mobile-bed model SRH-2D (Lai 2008; Lai 2010) with the slope stability model BISHOP (Mahdi 2004; Mahdi and Merabtene 2010) and the riverbank failed materials redistribution submodel REDISSED (Mahdi 2004). In the following, the models are presented first, and their coupling is then described and discussed.

SRH-2D Model

The SRH-2D (Sedimentation and River Hydraulics - Two-Dimensional) model (Lai 2008; Lai 2010) is a two-dimensional flow, mobile-bed and sediment transport model developed by the U.S. Bureau of Reclamation. The model is flexible; it uses an unstructured hybrid mesh numerical method that can be applied to arbitrarily shaped cells. Moreover, SRH-2D solves the 2D dynamic wave equations, i.e., the depth-averaged St. Venant equations, with a very robust and stable numerical scheme based on a finite volume discretization. In terms of hydrodynamic modeling capabilities, SRH-2D has shown its capacities for hydraulic calculations compared to Hydro_As-2D (Lavoie and Mahdi 2017) and was previously tested successfully in many other studies (Lai et al. 2010; Lai et al. 2016; Moges 2010).

For a complete analysis within SRH-2D, the model needs a mesh generator. Since the model adopts the arbitrarily shaped mesh system, any 2D mesh generator program may be used. At present, SRH-2D uses the SMS model (AQUAVEO 2019) as the mesh generator and postprocessing graphical model. A typical modeling consists of delimiting the initial solution domain on the SMS, defining the topographic and bathymetric data, assigning the channel's materials and boundary conditions and finally generating the mesh. Within the SMS, it is possible to run SRH-2D for single simulation or to export all the simulation data into files for future use, an approach that will be adopted in this study. The authors will use the exported data to launch the SRH-2D processor (*srh-2d*). The model outputs the results files that describe the time-dependent evolution of the cross-sections. Several forms of data processing can be considered.

BISHOP Model

BISHOP is a geotechnical stability analysis model developed by (Mahdi 2004) to evaluate bank profile stability. The model iteratively calculates the minimum factor of safety based on Bishop's modified method

(Philiponnat and Hubert 1979); it isolates the global minimum factor of safety from all the local minima for a given slope. Stability analysis is carried out based on the approach of circular failures, a type of riverbank failure often noticed *in situ* (Highland and Bobrowsky 2008; Philiponnat and Hubert 1979) and associated with cohesive soils (Thorne 1982). BISHOP has been tested and compared previously to other commercial rotational failure software (GeoSlope SLOPE/W) (Fredlund 1995) and has proven its ability to accurately evaluate the force equilibrium factor of safety for rotational failures (Mahdi 2004; Mahdi and Merabtene 2010). The geotechnical model iteratively calculates the minimum factor of safety based on Bishop's modified method (Philiponnat and Hubert 1979) by solving the following implicit equation:

$$FS = \frac{\sum_i^N \left(\frac{(W_i - u_i b_i) \tan \emptyset'_i + c'_i b_i}{\cos \alpha_i + \sin \alpha_i \frac{\tan \emptyset'_i}{FS}} \right)}{\sum_i^N (W_i \sin \alpha_i)} \quad (1)$$

In the above, FS is the factor of safety, and banks are considered unstable when $FS < 1$, and for any slice i (Fig. 1), W_i is the weight; b_i is the river width; u_i is the pore water pressure at the bottom of the slice; α_i is the angle between the vertical and the radius R of the circular slip surface; c'_i is the effective cohesion and $\emptyset'_i$is the effective angle of friction. In Fig.1, H refers to the horizontal interslice force, and I represents the center of a trial circle of radius R.Interested readers can refer to (Mahdi 2004; Mahdi and Merabtene 2010) for further details concerning the numerical implementation.

BISHOP combines the bank geometry and bank soil geotechnical properties (effective cohesion, undrained cohesion, interior effective friction angle, and saturated unit weight) in the same input file. One to nineteen stratigraphic layers might be defined for each riverbank, with each layer having its own geotechnical properties as well as pore water pressure conditions. In addition, the model can be adjusted when applied to a watercourse submerged by water; it takes into account the hydrostatic water pressure by assuming the surface water as a soil layer of unit weight equal to that of water but with no shear strength.

184 The BISHOP model was mainly used in the study instead of conventional software (i.e., GeoSlope,
185 SLOPE/W) to facilitate the automatic coupling of the models. In fact, the conventional software were
186 avoided since they require the model user to draw the bank profile and its different geotechnical layers as
187 well as the groundwater table, which is impractical in this study since many hydraulic cross-sections must
188 be analyzed during the flooding event which will be tedious and time consuming to do for each riverbank.

189 **REDISSED Submodel**

190 REDISSED is a sediment redistribution submodel developed by (Mahdi 2004) to reshape the bank
191 profiles following a circular failure. The model conserves the mass and accommodates the observed
192 failure form of the banks in the study site. In the case of bank failure, the model redistributes the bank-
193 derived materials in the flow section where their erosion and/or transport will be determined by the
194 subsequent hydraulic conditions incorporated in the mobile-bed model.
195 As stated above, since there is no consensus among researchers regarding the redistribution of the
196 derived bank materials (Darby and Delbono 2002; Nagata et al. 2000; Pizzuto 1990), the authors
197 considered a field-based approach implemented in the REDISSED submodel. It consists of redistributing
198 the failed materials as follows: The initial bank geometry is first described by a set of points (mesh nodes);
199 for simplification purposes, we consider the points ABCXZ plotted in Fig. . In the case of bank failure, the
200 circular sliding surface is along points ADC. The ABCD block is rotated so that the difference in altitude
201 between A and its image A' will be equal to H/α, where H is the failure height (the difference in altitude
202 between points A and C) and α is a coefficient greater than unity and is specified by the user based on
203 observations of the study site. Point B', the image of B, is projected orthogonally to obtain point B'' as
204 shown in Fig. .
205 Fig. illustrates the new bank profile defined by the points AA'B''C'EZ, where point E belongs to section
206 XZ, so that A'B'C'B''A' and CC'EXC have equal areas for mass (or area) conservation purposes.
207 In a nutshell, the slump blocks undergo a rotation followed by a translation that moves the upper end of
208 the sliding bank to the bottom of the cross-section while conserving the mass. Once the submodel
209 redefines the form of the failed blocks, the topography of the bank section is automatically updated
210 accordingly before moving on to the next hydraulic time step. Meanwhile, the geotechnical layers are

updated through linear interpolation assumptions between the different points defining the geotechnical layers.

Sliding cone area

Redistribution of the mass wasting deposits of the unstable talus will be performed by using REDISSED (Mahdi 2004) along the predefined cross-sections. However, the unstable failure block is a 2D planar surface. Hence, to ensure the fully two-dimensional aspect of the study, the authors considered a sliding bank area in the shape of a right cone with its axis as the cross-section line, its vertex as the upper point of intersection between the riverbank and the slip circle computed by BISHOP (Mahdi 2004), and its opening angle is a user-defined parameter (Fig.). The mesh nodes located within the sliding cone area will have their topography automatically interpolated to accommodate the new reshaped bank profile. The mesh nodes affected by the failure will have a vertical displacement according to their position with respect to the new bank geometry, i.e.,

$$Z_M = Z_{B''} + \frac{d_M}{d} \times (Z_{C'} - Z_{B''}) \quad (2)$$

where Z_M is the mesh node elevation obtained by interpolation; $Z_{B''}$ and $Z_{C'}$ are the elevations of the mesh nodes B'' and C', respectively, belonging to the new bank profile; d_M is the distance from the node B'', the nearest mesh node from node M; and d is the distance between the two mesh nodes B'' and C'.

The choice of the mesh nodes to be used for interpolation is done automatically, and the x coordinate of the interpolated mesh node (M) should be between the abscissa of the two mesh nodes, here nodes B'' and C'.

Coupling SRH-2D and BISHOP-REDISSED

The coupling between models started by incorporating bathymetric and topographic data on the SMS in a similar fashion to the conventional mobile-bed and sediment transport modeling with SRH-2D, and defining the cross-sections where the stability analysis will be performed. They will be set as node strings on the SMS just before generating the mesh (Fig.). Aftergenerating the mesh (Fig.) and assigning the

boundary conditions, the pre-established cross-sections will be defined as monitor lines (maximum of 98 monitor lines) to get access to their nodes when exporting data. All other necessary modeling inputs (Manning's roughness, materials, simulation time, and initial conditions) can be fixed; thereafter, the key simulation data can be exported to three principal files, the most important of which holds the node coordinates at the monitor lines. This file will be used to ensure automatic feedback between the vertical changes predicted by the 2D mobile-bed model and the lateral changes predicted by the geotechnical-stability and sediment-redistribution model BISHOP-REDISSED.

Assessing the geotechnical stability of the riverbanks and updating automatically the flow-wise 2D geometry in case of bank failure for a long-reach-scale system without having to manually move the mesh is seen as a key contribution of this study. Significant effort was expended to find a suitable procedure to model hydraulic cross-sections while considering their geotechnical characteristics. Herein, each cross-section was modeled as a set of vertical lines whose abscissa are the mesh nodes defining the transects. These vertical lines form points of intersection at each change in the geotechnical properties of the predefined layers (Fig.). Thus, two text files are used in compiling geometric and geotechnical data. The geometric file stores data in a vector whose components are the x-coordinate of the vertical line, the elevation of the highest point of the cross-section and the elevation of the base of the different geotechnical layers. We note that it is also possible to include the elevation of the crevice if it exists and the elevation of the water level in it. Similarly, the geotechnical file regroups the geotechnical properties of each soil layer for each riverbank profile separately, which includes the values of the effective cohesion c', the undrained cohesion c_u, the unit weight γ' and the interior effective friction angle $\emptyset'$ as well as the elevation of the groundwater table or the pore pressure ratio r_u. It is worth mentioning that the global coordinates of the nodes of the mesh in the SMS will be automatically transformed, translated and rotated to have local coordinates with an origin at the far-left bank node of each cross-section (Node 1 in Fig.). These coordinates will be used to define the geometric files for BISHOP model. This is a fundamental and necessary step since it will avoid distortion when updating the mesh and yet allows consideration of river sinuosity.

Having defined the hydraulic and geotechnical parameters, the next step consists of launching the developed automation algorithm. With a text-based interactive user interface, the user defines the case name, the number of cross-sections, the slope of the potential sliding cone and finally the time step Δt' to test the stability of the banks (Fig.). The developed algorithm, which uses, inter alia, an AutoHotkey script, will automatically launch the *srh-pre* and inputted SMS-exported files. The preprocessor stage will first check the possible errors and then output a directory file that contains the entire model input information, especially the topography. That file will be used to launch the processor *srh-2d* automatically. However, prior to that, the automation algorithm will make two principal modifications:

(1) The initial start time, time step and end time are among the simulation information stored on the directory file. The initial simulation end time will be automatically changed to the BISHOP time step Δt'. In addition, for the first run, the initial start time will be kept unchanged. However, starting from the second run, the start time will be the end time of the previous simulation, and the new end time will be Δt' plus the start time. The simulation will accordingly last Δt' of the flood event for each run. The algorithm will call up the BISHOP model (Mahdi 2004) to evaluate the bank stability at the end of each run. The program will launch SRH-2D several times (Nb_{times}) and test the bank stability at the end of each run until the total number of times is equal to the ratio between the initial end time and the BISHOP time step Δt' (Nb_{total}). It is worth noting that the chosen time step Δt' should preferably be a divisor of the initial end time if not the hydraulic time step.

(2) In addition to time information, the directory file records the name of the restart file, a file created by the SRH-2D model in a previous simulation using the same mesh and hydraulic conditions. The name of the file will be changed to the case name followed by _RST1. During each SRH-2D simulation, the restart file is generated at each interval specified within the model control. Herein, this file will be generated only at the end of each run and will be used as the initial condition of the next simulation. This allows a continuation from the end of the previous simulation and thus takes into account the last hydraulic-sediment transport conditions.

Following these few changes in the directory file, the program will launch the SRH-2D model for the first run. The vertical model proceeds in its own time until it reaches the bank time step, when the BISHOP model is activated. The SRH-2D model outputs a results file that describes the time-dependent evolution of the cross-sections. The developed program will compare the node elevations of the cross-sections with the initial elevation. In the absence of erosion, the analysis is advanced for the next time step, as illustrated in the flowchart (Fig.). If erosion occurs, at least around one riverbank, the new sections representing the bed at the end of the time step are tested for the stability of their banks. The new cross-sections will be divided into two riverbanks from the lowest bed elevation (Node 6 in Fig.). Each bank will be subsequently coupled with its corresponding pre-established geotechnical properties files to define the input files for BISHOP. Hence, the stability of the riverbank will be assessed; it will be performed under drained conditions for the first potential bank failure and under undrained conditions afterwards. In fact, after the first failure, the stability analysis will be performed using the resistance of the shear stress of the undrained materials. This is due to the decrease in the interstitial pressure that allows the bank to resist geometric changes over a certain timespan (Mahdi and Merabtene 2010) and then accounts for the protection afforded by the failed materials.

In the absence of rupture (FS>1), the simulation is advanced for the next time step (Fig.). Otherwise, the bank profile will be reshaped based on the REDISSED (Mahdi 2004) submodel; the corresponding geometric file will be updated to account for the new bank profile. Although the program will renew the channel bed and bank topography based on the updated geometry, prior to that, the program will make necessary transformations (translation and rotation) to adapt the new node coordinates to their initial global system on the SMS. In addition, the bed topography of all the nodes located inside the sliding cone area will be automatically interpolated to accommodate bank failure as illustrated in figure 9; the mesh will therefore be updated before moving to the next hydraulic time step.

Once the bed topography is updated, the program will set the restart file as an initial condition to continue from the last hydraulic-sediment transport conditions and ultimately make necessary changes in the start and end times, as explained before. The simulation will run as many times as necessary until the initial end time is achieved (see the application section below).

Application: case study

The approach adopted to verify the coupling procedure was applied over a long-reach scale; 7 kilometers of river length extending from the Première Chute Dam to Lake Témiscamingue along the Outaouais River at Notre-Dame-du-Nord, Quebec, was considered. The study reach is characterized by the presence of cohesive sediments along the river, and the height of the local banks typically vary between 35 m high near the dam and 15 m high at the entrance of Lake Témiscamingue. It is an interesting field site since the water never overflows, even in the case of dam failure; therefore, bank failures are the only risk for the riverside population.

Model setup

A 2D mesh initial solution domain representing the initial channel topography of the study area was prepared in the SMS. The solution domain includes the positions of the selected cross-sections, where the geotechnical stability analysis will be performed, modeled as straight segments moving downstream from right to left, where the 2D mesh node coordinates define the bank face geometry. Herein, 52 irregularly spaced cross-sections were selected (including inlet and outlet transects), as shown in Fig. . The cross-sections were carefully chosen to consider the hydraulic features of the channel, they relatively represent the field domain as they present the same soil characteristics and riverbank slopes around them from field observations.

A time series discharge with a peak of approximately 9780 m^3/s, which corresponds to the dam failure scenario, was imposed upstream (Fig.). A constant surface elevation of 179 m was enforced downstream that corresponds to the water elevation in the lake. To represent the bed behavior, a constant Manning's roughness coefficient (n) of 0.040 (d_{50}=160 mm) was used for the entire reach; it was estimated based on field observations in 2002 (Thibault, 2002); no calibration was needed. The sediment transport computation was carried out by using the Yang formula (Yang 1973), which is compatible with the bed material of the reach, which was assumed to be made of the same material as the riverbanks. Note, however, that the selection of the sediment transport equation is not important for the analysis below. Table 1 lists the grain size composition of the bed and bank material segregated into seven size classes

supported by SRH-2D (Lai 2010). The volumetric compositions considering the seven classes listed in Table 1 are 80%, 7%, 7%, 4%, 1%, 0% and 0%.

The geotechnical input parameters were prepared for each bank profile separately (104 bank profiles). They consist of a single homogeneous cohesive layer with measured properties supplemented by field test results carried out on some collected samples: effective cohesion c' =1.6 KPa; undrained cohesion c_u = 9 KPa; unit weight γ' = 18.6 KN/m^3; and interior effective friction angle $\emptyset'$ =32°. The pore pressure ratio, the ratio of the pore water pressure to the overburden pressure, was set to its maximum value r_u= 0.45 (Fredlund and Barbour 1986). In this regard, we emphasize that within BISHOP (Mahdi 2004; Mahdi and Merabtene 2010), it is also possible to define pore water pressures given the pressure field or the groundwater table. Since information was not available, we assumed the most unfavorable case and chose the maximum pore pressure ratio.

The coupling procedure between SRH-2D (Lai 2010) and BISHOP (Mahdi 2004) was applied for 9 hours of the event. The flow, sediment transport and bed evolution time step was set to 5 s, whereas the stability analysis was carried out each $\Delta t'$ =0.125 h. The time scale to assess the geotechnical stability of the banks is usually much greater than the time scales of hydrodynamic and channel bed morphological evolution. A sensitivity analysis will be conducted later to explore the impact of the time scale on the results of the model. Given the above values, the simulation will run 72 times (Nb_{total}= $9/(\Delta t')$= 72), and at the end of each run, the stability analysis will be assessed profile by profile. As stated earlier, to update the flow-wise 2D geometry, a cone-shaped failure block was considered. Since there are no available measured data regarding the extents of the failed area and because the mesh is relatively coarser, a 60° opening cone angle was assumed in the case of bank failures. Finally, the REDISSED parameter α was set to 5.5 as suggested by (Thibault C et al. 2002) to represent the form of the failed banks at the study site.

Results

Two different scenarios were simulated. The first scenario considered only vertical erosion modeling using the SRH-2D (Lai 2010) model, and the second scenario combined vertical and lateral erosion modeling using the coupling procedure. **Error! Reference source not found.** shows the initial and final

profiles for selected riverbanks considering both scenarios, Fig. 13 shows the bank retreat plan view and Fig.14 shows a 3D view of a redefined bank profile. The evolution of the factor of safety for the riverbanks during the simulation period is illustrated in **Error! Reference source not found.**. Furthermore, the predicted net bank retreat distances for all the cross-sections are displayed in Fig. .

These results show that bank failures are mostly observed alongside the bend and in the upstream section above it, where banks are high and steep. The bank retreat process was particularly significant within the river bend, which reveals a bank retreat up to 6 m for cross-sections 13 to 16, particularly on the right bank section (Fig.). This can most likely be attributed to the optimal combination of slope and flow, to similarities in bank geometry and to the relatively narrower cross-sections in that area. In fact, fluvial erosion seems to have contributed more to steepening the bank profiles upstream, making them susceptible to geotechnical failures. Downstream, bank failures were almost absent, flow velocity and shear stress were smaller, bank heights and slopes were lower, and the channel morphological changes were then exclusively dominated by fluvial erosion.

Moreover, the erosion of the channel bed is noticeably stronger when exhibiting the bank failure process, especially for the first cross-sections (7R, 9L, and 9R) (hereafter denoting L for the left bank and R for the right bank) and along the bend (10L,10R and 14R). The failed bank-deposited materials downslope seem to serve as temporary protection from the fluvial erosion but make the cross-sections narrower and the slopes steeper, which increase the speed of the flowing water and the channel bed erosion rate. Furthermore, this rate appears to be related to the timing of the mass failure. In fact, the channel bed zone of the transects where the banks were predicted to fail early have been eroded more (9L, 14R, 23R and 28L) compared to those that failed later (1R and 9R) where the simulated bed deepening is approximately the same when considering the fluvial erosion only. This may be justified because the bank predicted to fail earlier becomes much more stable over the rest of the simulation period, which makes the channel narrower for a long period. Indeed, after the first bank failure, we hypothesize that bank stability will be evaluated with undrained conditions, which enhance the geotechnical stability of the bank. In addition, as stated above, the protection afforded by the failed materials further increases their stability, as the failed materials have to be removed first by fluvial erosion. Together, these findings explain the

394 slightly higher channel bed erosion rate for banks predicted to fail earlier compared to those that failed
395 later.

396 Furthermore, after the bank failure, we note that the bank geometry was reshaped, and the failed blocks
397 were redistributed along the cross-section. The redistribution of the eroded materials is clearly visible for
398 the banks that failed later (1R and 9R) since the fluvial erosion did not consume all the material deposits.
399 However, the volume of the failed bank materials is seen to be reduced for banks that failed earlier (14R,
400 23R). In addition, the slump blocks have been redistributed all around the neighboring transects
401 considering the failure cone shape assumption established in the process of this study. Fig. shows the
402 bank geometry profile of the cross-sections neighboring the failed bank at cross-section 10, where the
403 bed elevations of the mesh nodes were displaced to account for the newly defined bank profile.

404 **Sensitivity to the BISHOP time step**

405 Sensitivity analysis was completed to determine the impact of the geotechnical stability analysis time step
406 on the bank failure prediction and retreating distances. Simulations with different time steps were run
407 using 0.0625, 0.125, 0.25 and 0.5 h. The selected time steps are all divisors of the simulation total time (9
408 hours) to ensure having the necessary runs to reach it. Hence, the simulation was run 144, 72, 36 and 18
409 times for each time step. By doing so, we reasonably hypothesize that the closer the BISHOP (Mahdi
410 2004) time step is to the SRH-2D (Lai 2010) time step, the more we are certain to capture all the potential
411 riverbank failures.
412 Fig. shows the retreating bank distances for the right and left top bank lines for different geotechnical
413 time steps. Table 2 lists only riverbanks that were predicted to fail for certain time steps but not for others.
414 As expected, more banks were predicted to fail while decreasing the BISHOP (Mahdi 2004) time step. In
415 fact, the right bank at cross-section 7 and the left bank at cross-section 28 were predicted to fail for both
416 time steps 0.0625 and 0.125 h but not for the highest time steps. Three and even four bank failures were
417 missed for time steps of 0.25 and 0.5 h; the flow conditions have perhaps changed, and the banks are no
418 longer unstable. However, we note that the left bank at cross-section 9 was predicted to fail when
419 considering time step 0.125 but not time step 0.0625. This can be attributed to the BISHOP (Mahdi 2004)

order of accuracy. Fig. shows that the factor of safety was very close to unity; to three decimal places, the bank was considered, though, stable.

Moreover, the timing of bank failure seems to be accurately predicted using small time steps (0.0625 and 0.125). Fig. shows the evolution of the factor of safety at the left bank of cross-section 10 considering the four configurations. The failure occurs 2.375 hours from the start of the simulation when using time steps of 0.0625 and 0.125 h. However, the riverbank was predicted to fail later for the two other time steps (almost one hour later). This can most likely be justified by the subsequent failures along the directly neighboring transects of the channel bank. In fact, the left bank of transect 9 was predicted to fail 2 hours after the simulation begins when using 0.0625 and 0.125 time steps but not for the highest time steps. This probably impacted the 10L bank failure time when using 0.25- and 0.5 time steps, as the channel bank form in that area was different. Although the 10L bank profile was slightly the same for the four different time steps (not shown), the difference between the timings was insignificant compared to the total remaining time of the simulation.

Overall, despite the timing issues highlighted above, we notice that the predicted bank retreat area and the retreating bank distances were considerably close for the small time steps (Fig.). The model was nevertheless capable of capturing the potential troubling spots without regard to the chosen time step. We recommend, however, using small time steps to improve predictions of the retreat location with respect to the computational cost of the simulation.

Discussion

Despite the overall success in predicting the bank retreat and redistributing the removed unstable failure blocks, some aspects of the study need more attention. First, the predicted bank retreat depends on the mesh size considered. With the current mesh, the bank zone is badly represented, an average of ten lateral nodes define the transects, which unsatisfactorily capture the bank face geometry and would yield to a scarce bank retreating prediction. Second, after bank failure, only a few neighboring cross-sections were reshaped to account for the newly defined bank profile, perhaps because of the cone interior angle and again the mesh density. Indeed, we used a relatively coarser mesh, and few elements were affected. The mesh was locally refined at cross-section 10 to take account of the newly reshaped bank profile as

illustrated in Fig. 20; further mesh refinement may allow defining the sliding area accurately but increases the study computational cost and may induce model divergence, as the mesh representing the failed banks might be distorted considerably. The cone interior angle considered could affect the extent of the sliding area, especially for a much-refined mesh. The angle of 60° was set as an assumption in the present study, a sensitivity analysis might be conducted to evaluate the influence of the angle but it is outside the scope of this research. Third, after bank failure, the REDISSED (Mahdi 2004) submodel reshapes the bank profile as described in detail earlier, although the submodel adds some supplementary points to correctly represent the geometry of the bank face toward ensuring mass conservation. However, the elevation of those additional points will be used to shift the mesh node elevations using a simple linear interpolation method, which may induce loss of precision. Higher-order interpolation functions could potentially yield better accuracy but were abandoned during the study since it would be reasonable and suitable to combine the functions with a much finer mesh. Fourth, the fluvial erosion rate before and after the bank failure was considered the same, which might be incorrect as the critical shear stress of the materials differs, but this was also an assumption that we have made in the present research, which seems to be acceptable since it does not affect the objectives of the study. Finally, the pore pressure ratio was considered constant for all the banks, which might influence the bank failure prediction since cohesive banks are more susceptible to failure during rapid-drawdown, high-flow events (Alonso and Pinyol 2016). The constant pore pressure ratio was again an assumption that we considered in the present study and might be a subarea for future improvement.

Streambank erosion modeling of the river reach extending from the Première Chute Dam to Lake Témiscamingue along the Outaouais River was very challenging. The reach longitudinal length was approximately 7 km, the banks are very tall and steep, and landslides along this river reach are the predominant existing risk. Simulation of the river reach evolution was conducted considering a dam break scenario that requires a frequent decrease in the hydraulic time step to ensure model convergence. Notwithstanding those difficulties, up to 100 m of bank retreat was predicted at several riverbanks (Fig.), and almost 20 cross-sections were reshaped using the developed coupling procedure. Typical results demonstrating the effectiveness of the developed methodology were presented in the study. Importantly, the model allows the automatic prediction of bank retreat due to both fluvial erosion and geotechnical

failure in long-reach-scale modeling systems using a 2D mesh in a simple and easy-to-use manner. Without survey data, the model is valid primarily for the identification of potential trouble spots for streams without necessarily requiring various input parameters.

Conclusion

In this paper, a new platform coupling a 2D mobile-bed modeling software, SRH-2D, a rotational failure analysis model, BISHOP, and a bank failure sediment-redistribution submodel, REDISSED, was developed. The major contributions are the redistribution of the slump blocks produced by riverbank mass failures onto the 2D mesh while conserving the mass; automation of the data exchanges between the different models, which makes the simulation less tedious; and finally, the robustness and ease of use of the model, which makes it applicable to practical stream events.

The developed coupling procedure has been applied to simulate the channel morphology of the Outaouais River at Notre-Dame-Du Nord; considering the complexities of the study site and the shortage of geotechnical and survey data, all four established objectives were nonetheless attained. The coupling approach showed encouraging results; up to 100 m of bank retreat was predicted, and the bank faces of over 20 cross-sections were renewed. However, the study can be further enhanced. In this field application, it has been noted that redistribution of unstable blocks is done merely along the failed banks, yet the bed elevations of only a few nodes of the neighboring cross-sections were updated. The study can accordingly be improved by integrating a more accurate submodel capable of evaluating the extent of the slumped area based on the real topography and soil properties, which could be an interesting area of future research. Moreover, given the influence of pore pressure on the factor of safety (Casagli et al. 1999), it would be beneficial to improve the BISHOP model by coupling it to a hydrogeological model giving the distribution of interstitial pressure in the soil instead of fixing a constant pore pressure ratio for all the riverbanks during the simulation period. Finally, nonfluvial processes such as seepage or rainfall events were not included in this study. Those processes could also impact the streambank erosion predictions; the fluvial process-based models alone are insufficient. Modeling those nonfluvial processes is another avenue for future research.

Acknowledgment

This research was supported in part by a National Science and Engineering Research Council (NSERC) Grant and *Hydro-Quebec.*

Notation

The following symbols are used in this paper:

b_i	Slice width
c'	Effective cohesion
c'_i	Effective cohesion of the slice
c_u	Undrained cohesion
d	Distance between two mesh nodes
d_{50}	Diameter at which 50% of a sample's mass is comprised of smaller particles
FS	Factor of Safety
H	The failure height
i	Slice
L	Left bank
Nb_{times}	Number of times to launch SRH-2D
Nb_{total}	The total number of times to launch SRH-2D
R	Right bank
r_u	Pore pressure ratio
u_i	Pore pressure ratio at the bottom of the slice

521 W_i Slice Weight

522 Z Mesh node elevation

523 α Coefficient greater than the unity, specified by the user based on field observation

524 α_i Angle between the vertical and the radius of the circular slipe surface

525 $\emptyset'$ Interior effective friction angle

526 $\emptyset'_i$ Interior effective friction angle of the slice

527 γ' Saturated unit weight

528 $\Delta t'$ Time step to test banks stability

529 **References**

530 Abad, J. D., and Garcia, M. H. (2006). "RVR Meander: A toolbox for re-meandering of channelized
531 streams." *Computers & Geosciences*, 32(1), 92-101.

532 Alonso, E. E., and Pinyol, N. M. (2016). "Numerical analysis of rapid drawdown: Applications in real
533 cases." *Water Science and Engineering*, 9(3), 175-182.

534 AQUAVEO (2019). "SMS 12.3 - The Complete Surface-water Solution.",
535 <http://www.aquaveo.com/software/sms-surface-water-modeling-system-introduction>. (June 10,
536 2019).

537 ASCE Task Committee on Hydraulics, B. M., and Modeling of River Width Adjustment (1998). "River
538 width adjustment II: Modeling." *Journal of Hydraulic Engineering*, 124(9), 903-917.

539 Casagli, N., Rinaldi, M., Gargini, A., and Curini, A. (1999). "Pore water pressure and streambank stability:
540 results from a monitoring site on the Sieve River, Italy." *Earth Surface Processes and Landforms:*
541 *The Journal of the British Geomorphological Research Group*, 24(12), 1095-1114.

542 Darby, S. E., and Delbono, I. (2002). "A model of equilibrium bed topography for meander bends with
543 erodible banks." *Earth Surface Processes and Landforms: The Journal of the British*
544 *Geomorphological Research Group*, 27(10), 1057-1085.

545 Darby, S. E., Rinaldi, M., and Dapporto, S. (2007). "Coupled simulations of fluvial erosion and mass
546 wasting for cohesive river banks." *Journal of Geophysical Research: Earth Surface*, 112(F3).

547 Fredlund, D. (1995). "User's guide SLOPE/W." *GEO-SLOPE International, Ltd., Calgary, Alb*.

548 Fredlund, D., and Barbour, S. (1986). "The prediction of pore pressure for slope stability analysis." *Proc.,*
549 *Slope Stability Seminar, Univ. of Saskatchewan, Saskatoon, SK*.

Galland, J.-C., Goutal, N., and Hervouet, J.-M. (1991). "TELEMAC: A new numerical model for solving shallow water equations." *Advances in Water Resources*, 14(3), 138-148.

Highland, L., and Bobrowsky, P. T. (2008). *The landslide handbook: a guide to understanding landslides*, US Geological Survey Reston.

Lai, Y. (2008). "SRH-2D version 2: Theory and User's Manual, Sedimentation and River Hydraulics–Two-dimensional River Flow Modeling." *US Department of the Interior, Bureau of Reclamation, Technical Service Center, Denver, CO*.

Lai, Y. (2017). "Modeling Stream Bank Erosion: Practical Stream Results and Future Needs." *Water*, 9(12), 950.

Lai, Y. G. (2010). "Two-dimensional depth-averaged flow modeling with an unstructured hybrid mesh." *Journal of Hydraulic Engineering*, 136(1), 12-23.

Lai, Y. G., Greimann, B. P., and Wu, K. (2010). "Soft bedrock erosion modeling with a two-dimensional depth-averaged model." *Journal of Hydraulic Engineering*, 137(8), 804-814.

Lai, Y. G., Smith, D. L., and Israel, J. (2016). "2D and 3D Flow Modeling of the Sacramento River Fremont Weir Section." *Proc., World Environmental and Water Resources Congress* 421-432.

Lai, Y. G., Thomas, R. E., Ozeren, Y., Simon, A., Greimann, B. P., and Wu, K. (2012). "Coupling a two-dimensional model with a deterministic bank stability model." *Proc., Proceedings of the ASCE World Environmental and Water Resources Congress, Albuquerque, NM, USA*, 1290-1300.

Lai, Y. G., Thomas, R. E., Ozeren, Y., Simon, A., Greimann, B. P., and Wu, K. (2015). "Modeling of multilayer cohesive bank erosion with a coupled bank stability and mobile-bed model." *Geomorphology*, 243, 116-129.

Langendoen, E. J. (2000). *Concepts: Conservational channel evolution and pollutant transport system*, USDA-ARS Naitonal Sedimentation Laboratory.

Langendoen, E. J., Mendoza, A., Abad, J. D., Tassi, P., Wang, D., Ata, R., El kadi Abderrezzak, K., and Hervouet, J.-M. (2016). "Improved numerical modeling of morphodynamics of rivers with steep banks." *Advances in water resources*, 93, 4-14.

Langendoen, E. J., and Simon, A. (2008). "Modeling the evolution of incised streams. II: Streambank erosion." *Journal of hydraulic engineering*, 134(7), 905-915.

Langendoen, E. J., Wells, R. R., Thomas, R. E., Simon, A., and Bingner, R. L. (2009). "Modeling the evolution of incised streams. iii: model application." *Journal of Hydraulic Engineering*, 135(6), 476-486.

Lavoie, B., and Mahdi, T.-F. (2017). "Comparison of two-dimensional flood propagation models: SRH-2D and Hydro_AS-2D." *Natural Hazards*, 86(3), 1207-1222.

Mahdi, T.-F. (2004). "Prévision par modélisation numérique de la zone de risque bordant un tronçon de rivière subissant une rupture de barrage [Prediction by numerical modeling of the risk zone bordering a section of river undergoing a dam break]."Ph.D. Thesis, Ecole Polytechnique de Montréal, Quebec, Canada.

Mahdi, T.-F., and Merabtene, T. (2010). "Automated numerical analysis tool for assessing potential bank failures during flooding." *Natural hazards*, 55(1), 3-14.

Mahdi, T., and Marche, C. (2003). "Prévision par modélisation numérique de la zone de risque bordant un tronçon de rivière subissant une crue exceptionnelle [Prediction by numerical modeling of the risk

591 zone bordering a section of river undergoing an exceptional flood]." *Canadian Journal of Civil*
592 *Engineering*, 30(3), 568-579.

593 Moges, E. M. (2010). "Evaluation of sediment transport equations and parameter sensitivity analysis
594 using the SRH-2D Model." Universität Stuttgart.

595 Motta, D., Abad, J. D., Langendoen, E. J., and Garcia, M. H. (2012). "A simplified 2D model for meander
596 migration with physically-based bank evolution." *Geomorphology*, 163, 10-25.

597 Nagata, N., Hosoda, T., and Muramoto, Y. (2000). "Numerical analysis of river channel processes with
598 bank erosion." *Journal of Hydraulic Engineering*, 126(4), 243-252.

599 Philiponnat, G., and Hubert, B. (1979). "Fondation et ouvrage en terre." *Eyrolles*, 19-20.

600 Pizzuto, J. E. (1990). "Numerical simulation of gravel river widening." *Water Resources Research*, 26(9),
601 1971-1980.

602 Rinaldi, M., Mengoni, B., Luppi, L., Darby, S. E., and Mosselman, E. (2008). "Numerical simulation of
603 hydrodynamics and bank erosion in a river bend." *Water Resources Research*, 44(9).

604 Rousseau, Y. Y., Van de Wiel, M. J., and Biron, P. M. (2017). "Simulating bank erosion over an extended
605 natural sinuous river reach using a universal slope stability algorithm coupled with a
606 morphodynamic model." *Geomorphology*, 295, 690-704.

607 Simon, A., Curini, A., Darby, S. E., and Langendoen, E. J. (2000). "Bank and near-bank processes in an
608 incised channel." *Geomorphology*, 35(3-4), 193-217.

609 Simon, A., Doyle, M., Kondolf, M., Shields Jr, F., Rhoads, B., and McPhillips, M. (2007). "Critical
610 Evaluation of How the Rosgen Classification and Associated “Natural Channel Design” Methods
611 Fail to Integrate and Quantify Fluvial Processes and Channel Response 1." *JAWRA Journal of*
612 *the American Water Resources Association*, 43(5), 1117-1131.

613 Simon, A., Pollen-Bankhead, N., and Thomas, R. E. (2011). "Development and application of a
614 deterministic bank stability and toe erosion model for stream restoration." *Stream restoration in*
615 *dynamic fluvial systems*, 453-474.

616 Thibault C, Leroueil S, and J, L. (2002). "Évolution des berges de rivière en cas de rupture de barrage:
617 cas du barrage Première-Chute." Université Laval, Québec.

618 Thorne, C. (1982). "Processes and mechanisms of river bank erosion." *Gravel-bed rivers*, 227-271.

619 Yang, C. T. (1973). "Incipient motion and sediment transport." *Journal of the hydraulics division*, 99(10),
620 1679-1704.

621 Yang, C. T. (1976). "Minimum unit stream power and fluvial hydraulics." *Journal of the hydraulics division*,
622 102(7), 919-934.

623 Yang, C. T., Trevino, M. A., and Simoes, F. J. (1998). *User's Manual for GSTARS 2.0 (Generalized*
624 *Stream Tube Model for Alluvial River Simulation Version 2.0)*, US Department of Interior, Bureau
625 of Reclamation.

626

627

Figures Captions

Fig. 1. Equilibrium of a soil layer (simplified Bishop method) (Mahdi 2004)).

Fig. 2. Initial geometry and circular failure (Scale-adjusted to display the details) ((Mahdi 2004)).

Fig. 3. Redistribution of the slump blocks following a circular failure (Scale-adjusted to display the details) ((Mahdi 2004)).

Fig. 4. Top view of the extents of the failed area defined within a cone-shaped form. The elevation of mesh nodes located in that area will be updated to account for the newly defined bank profile.

Fig. 5. The cross-sections before generating the mesh on the SMS.

Fig. 6. The cross-sections after generating the mesh on the SMS.

Fig. 7. The initial cross-section bed profile and the associated soil layers.

Fig. 8. The coupling procedure methodology.

Fig. 9. Sliding cone area and affected mesh nodes a) Plan view b) 3D view.

Fig. 10. The initial bathymetry for the Outaouais River at Notre-Dame-du-Nord, Quebec.

Fig. 11. The flood hydrograph at the upstream.

Fig. 12. The initial and final bank profiles for selected right and left riverbanks, and evolution of the factor of safety during the simulation period

Fig. 13. The predicted bankline changes after dam break occurrence (Red line) (retreats are 10 times exaggerated).

Fig. 14. The 3D view of a redefined bank profile.

Fig. 2. The predicted net bank retreat distances for all the predefined cross-sections.

Fig. 3. The left and right bank profiles for cross-sections upstream and downstream cross-section 10.

649 **Fig. 17.** The net bank retreat sensitivity to the BISHOP time step for the right and the left riverbanks.

650 **Fig. 18.** The evolution of the factor of safety of the right bank at cross-section 9.

651 **Fig. 19.** The evolution of the factor of safety of the right bank at cross-section 10 considering four different
652 geotechnical time steps.

653 **Fig. 20.** Sliding cone area and affected mesh nodes before and after refining the mesh for cross section
654 10.

655

Tables Captions

Table 1. Size ranges of seven sediment size classes used for the channel bed modeling.

Table 2. Riverbanks predicted to fail for different geotechnical time steps.

Table 3. Size ranges of seven sediment size classes used for the channel bed modeling

Sediment Size Class	Size Range (mm)
1	0.0025 to 0.0625
2	0.0625 to 0.125
3	0.125 to 0.25
4	0.25 to 0.5
5	0.5 to 1
6	1 to 2
7	>2

Table 2. Riverbanks predicted to fail for different geotechnical time steps. F: Failed banks; U: Unfailed banks.

BISHOP's time step(h)	Cross-sections																		
	1	6	7	9	10	11	12	13	14	15	16	21	23	24	25	26	27	28	29
0.0625	F	F	F	U	F	F	F	F	F	F	F	F	F	F	F	F	F	F	F
0.125	F	F	F	F	F	F	F	F	F	F	F	F	F	F	F	F	F	F	F
0.25	F	F	U	U	F	F	F	F	F	F	F	F	F	F	F	F	F	U	F
0.5	U	U	U	U	F	F	F	F	F	F	F	F	F	F	F	F	F	U	F

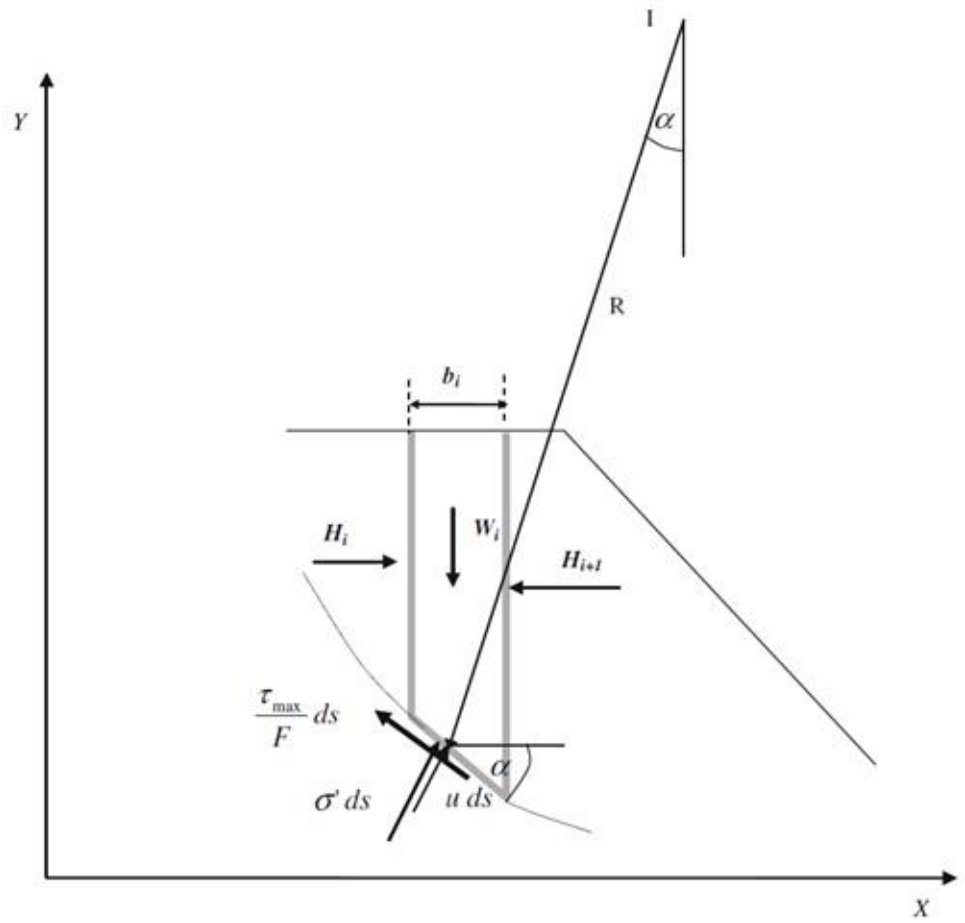

668

669 **Fig. 4**. Equilibrium of a soil layer (simplified Bishop method) (Mahdi 2004)).

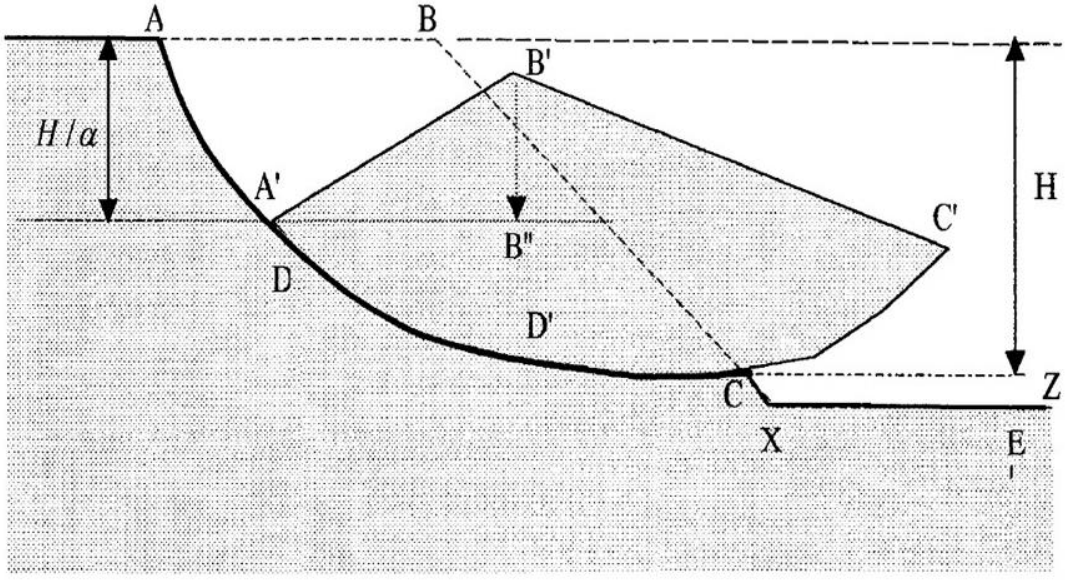

670

671 **Fig. 2.** Initial geometry and circular failure (Scale-adjusted to display the details) ((Mahdi 2004)).

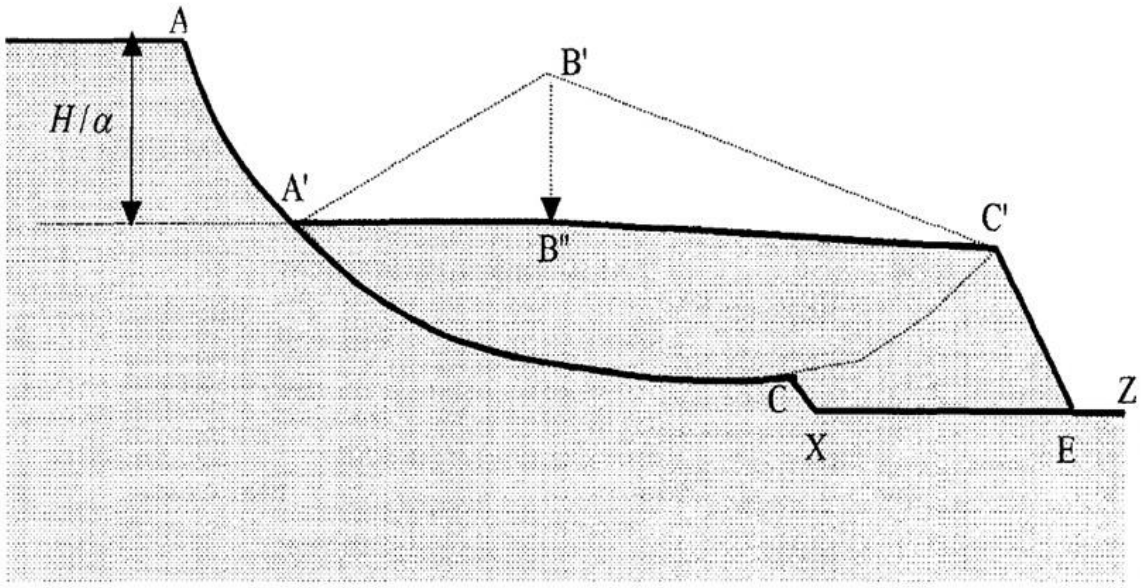

672
673 **Fig. 3.** Redistribution of the slump blocks following a circular failure (Scale-adjusted to display the details)
674 ((Mahdi 2004)).

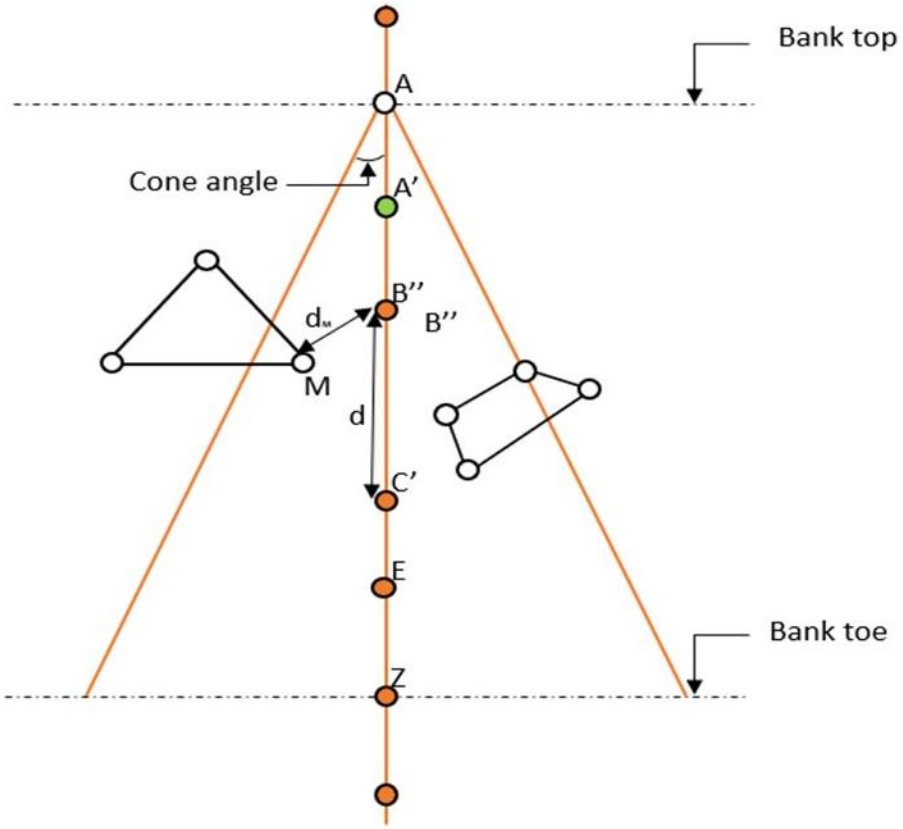

675

676 **Fig. 4.** Top view of the extents of the failed area defined within a cone-shaped form. The elevation of
677 mesh nodes located in that area will be updated to account for the newly defined bank profile.

678

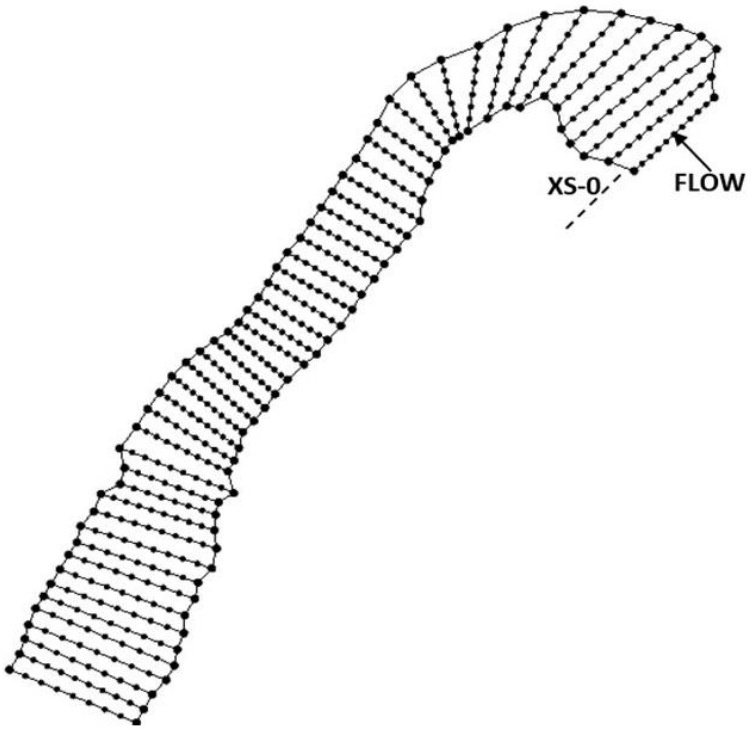

679

680 **Fig. 5.** The cross-sections before generating the mesh on the SMS.

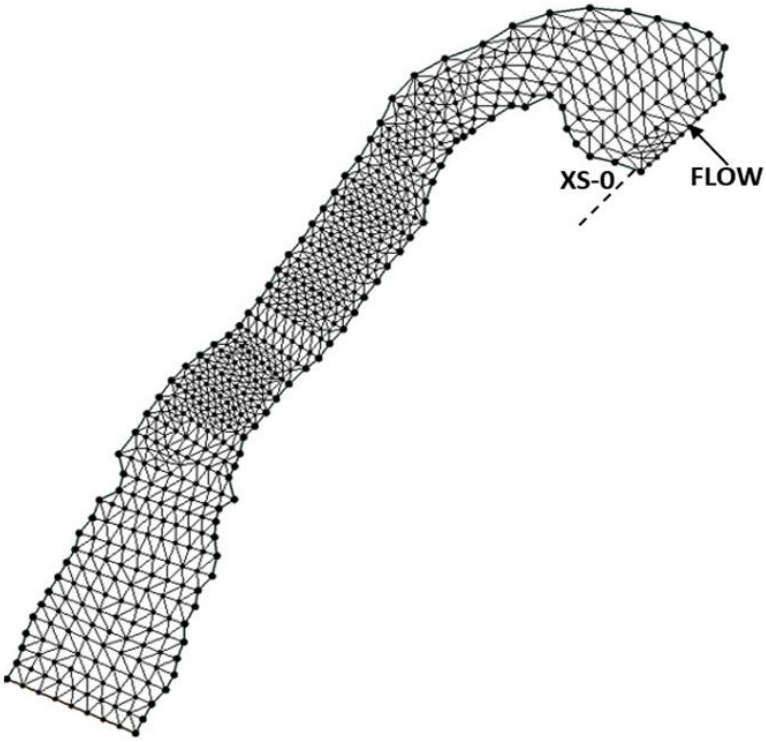

681

682 **Fig. 6.** The cross-sections after generating the mesh on the SMS.

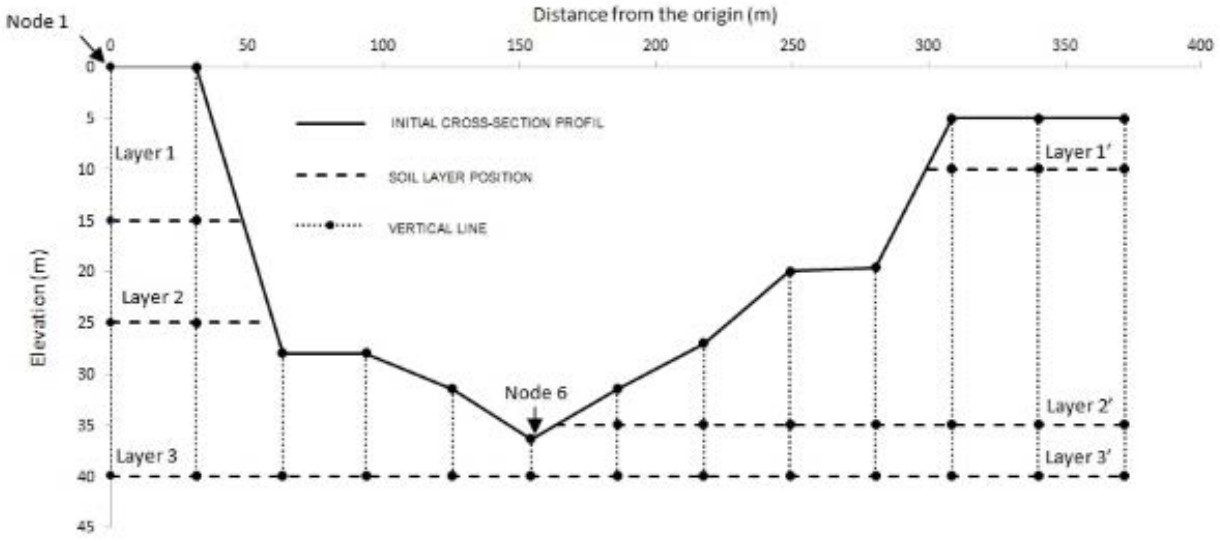

683

684 **Fig. 7.** The initial cross-section bed profile and the associated soil layers.

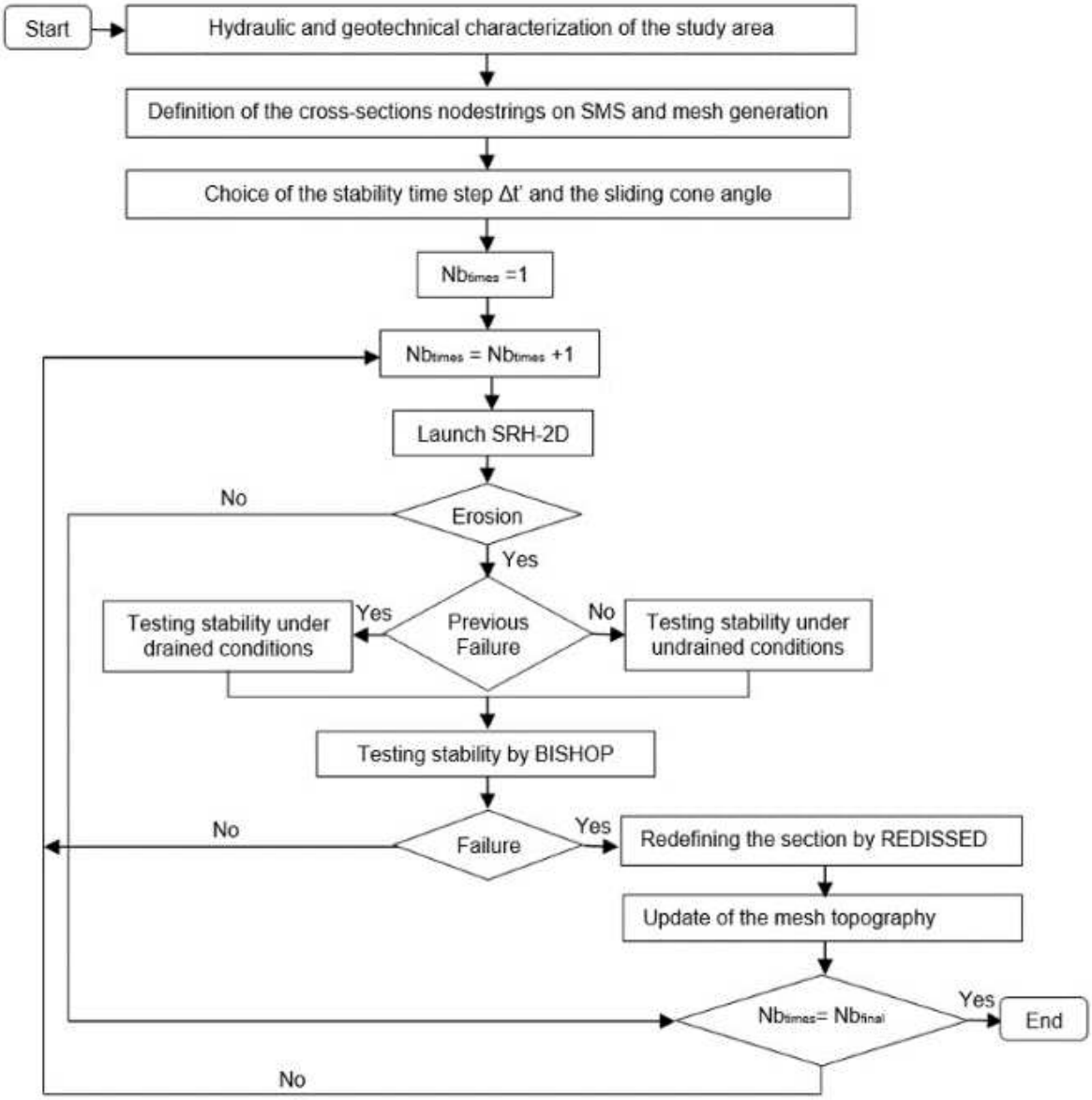

685

686 **Fig. 8.** The coupling procedure methodology.

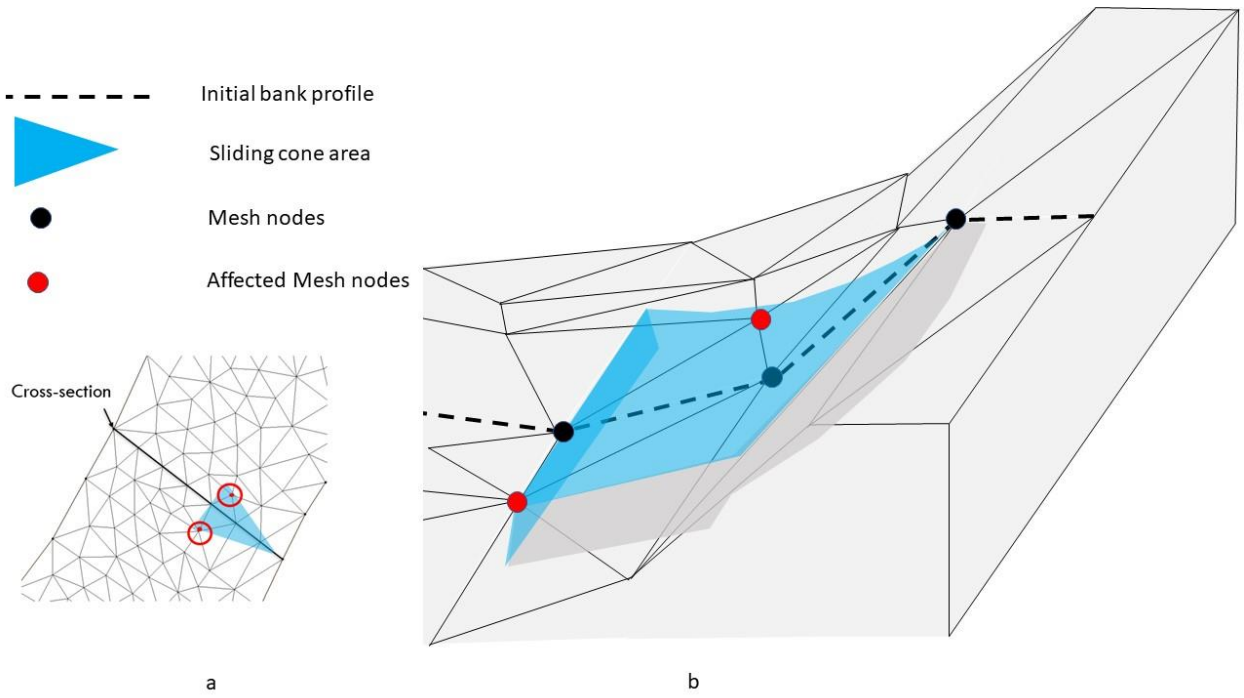

Fig. 9. Sliding cone area and affected mesh nodes a) Plan view b) 3D view.

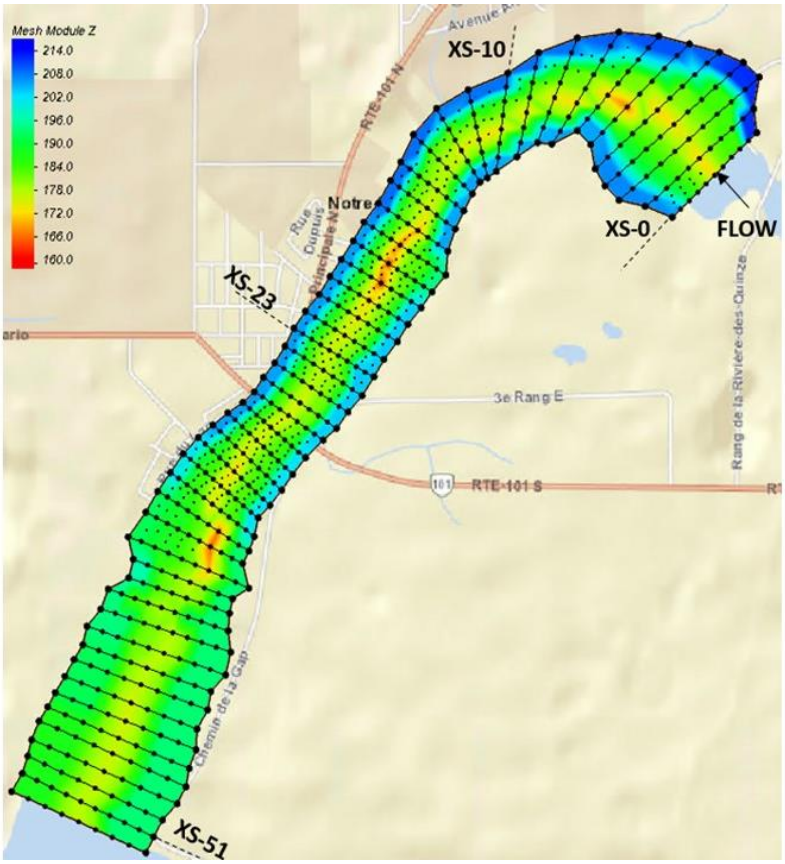

Fig. 10. The initial bathymetry for the Outaouais River at Notre-Dame-du-Nord, Quebec.

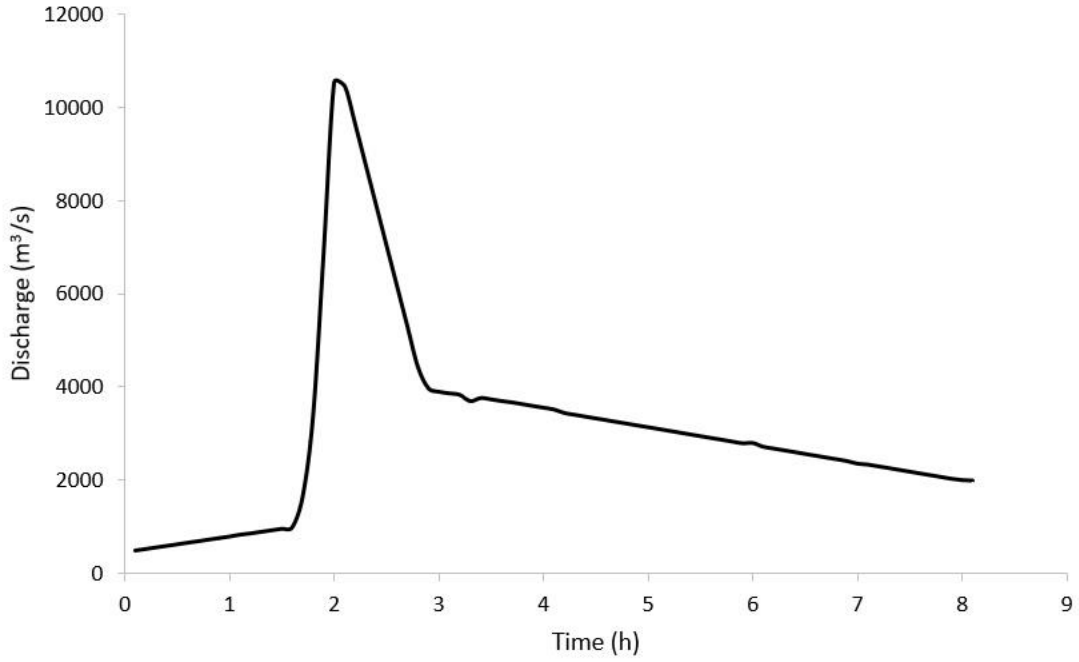

691

692 **Fig. 11.** The flood hydrograph at the upstream.

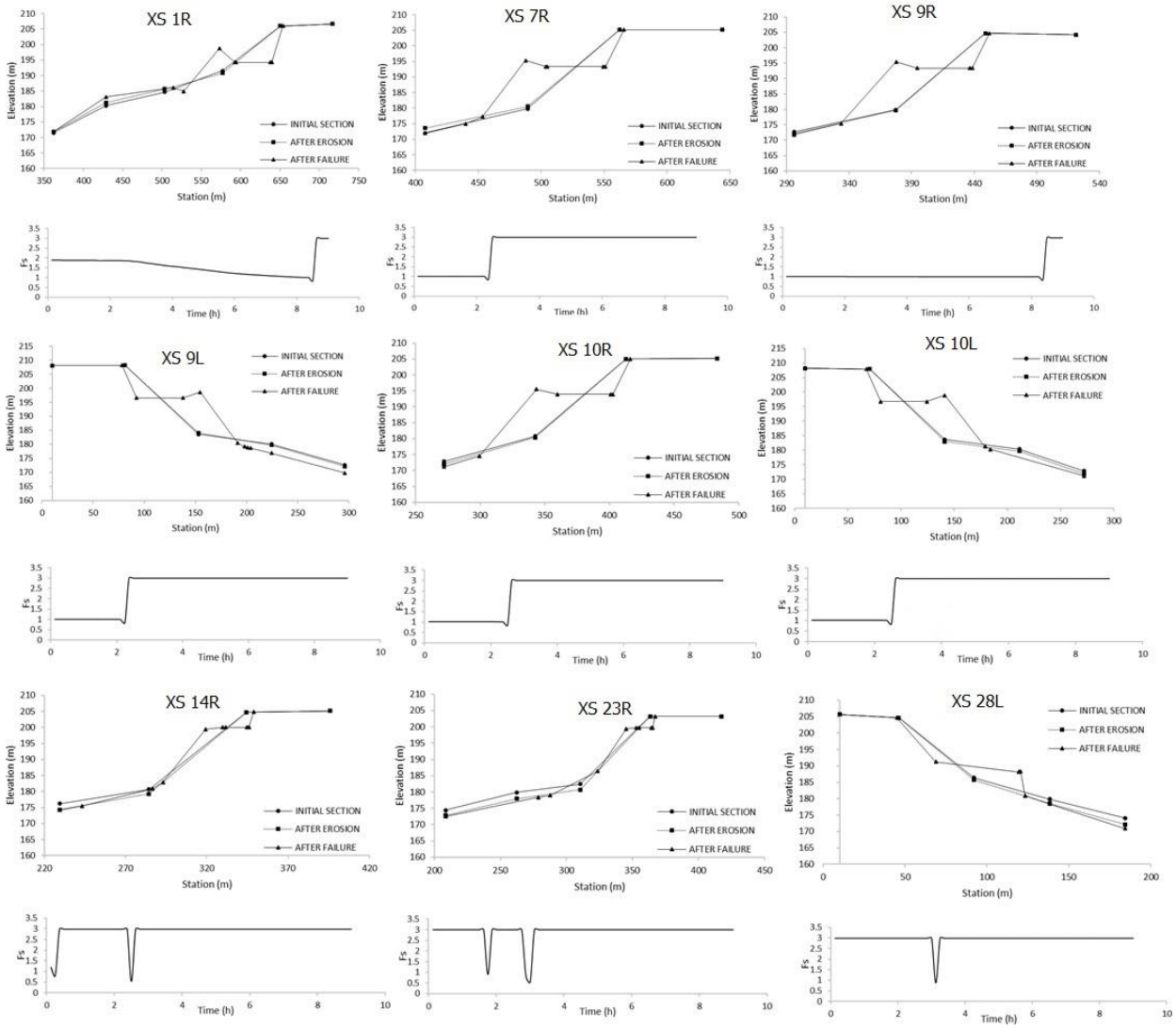

693

694 **Fig. 12.** The initial and final bank profiles for selected right and left riverbanks, and evolution of the factor
695 of safety during the simulation period

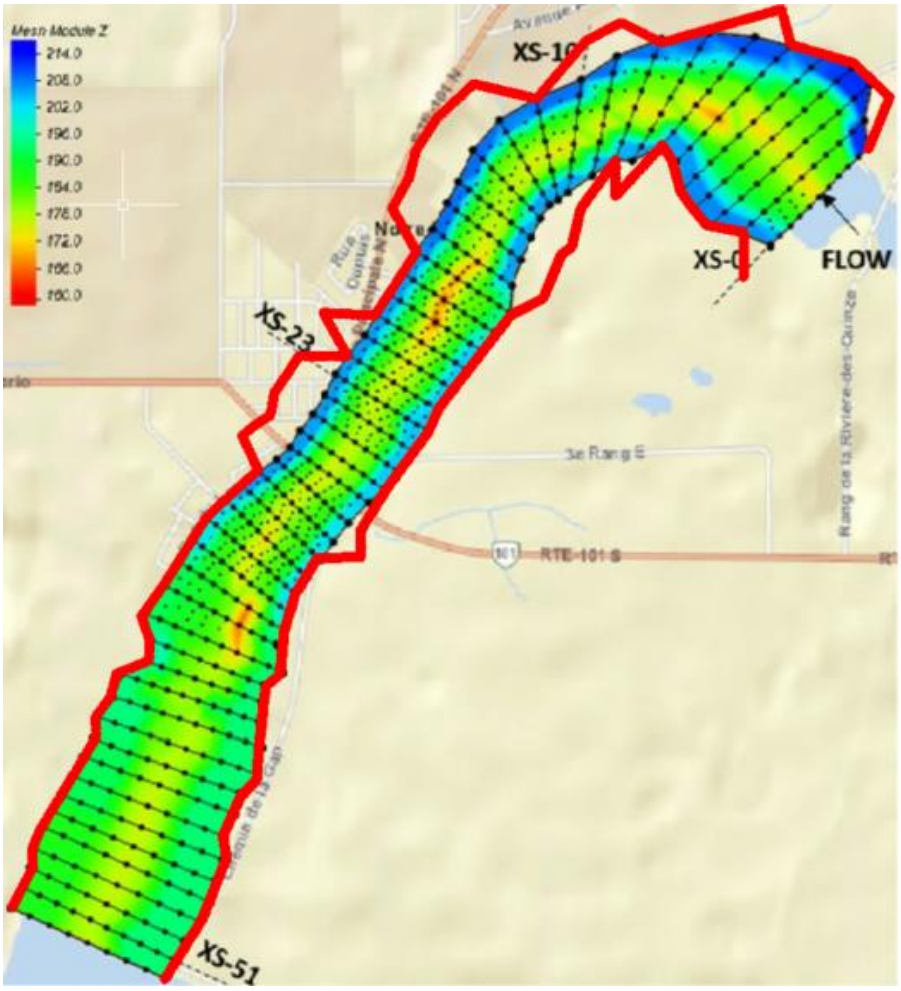

Fig. 13. The predicted bankline changes after dam break occurrence (Red line) (retreats are 10 times exaggerated).

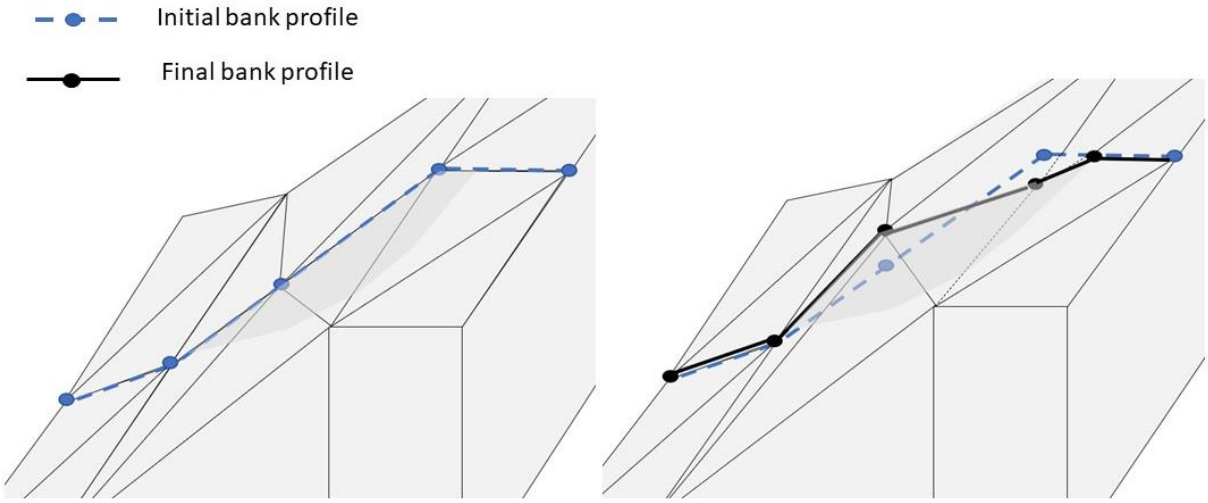

Fig. 14. The 3D view of a redefined bank profile.

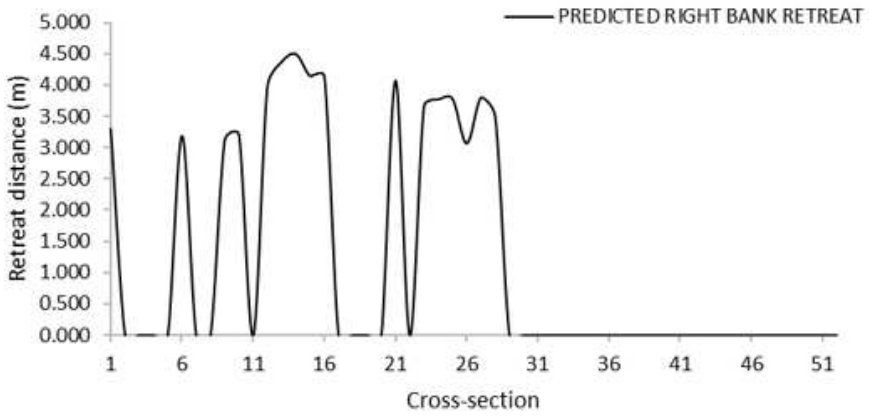

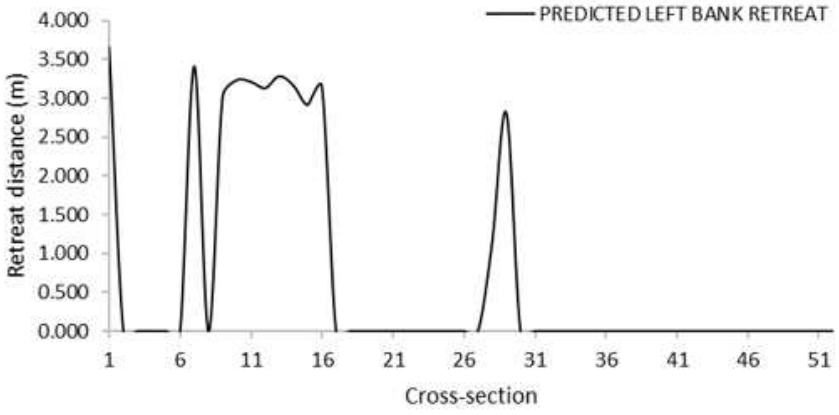

701

702 **Fig. 5.** The predicted net bank retreat distances for all the predefined cross-sections.

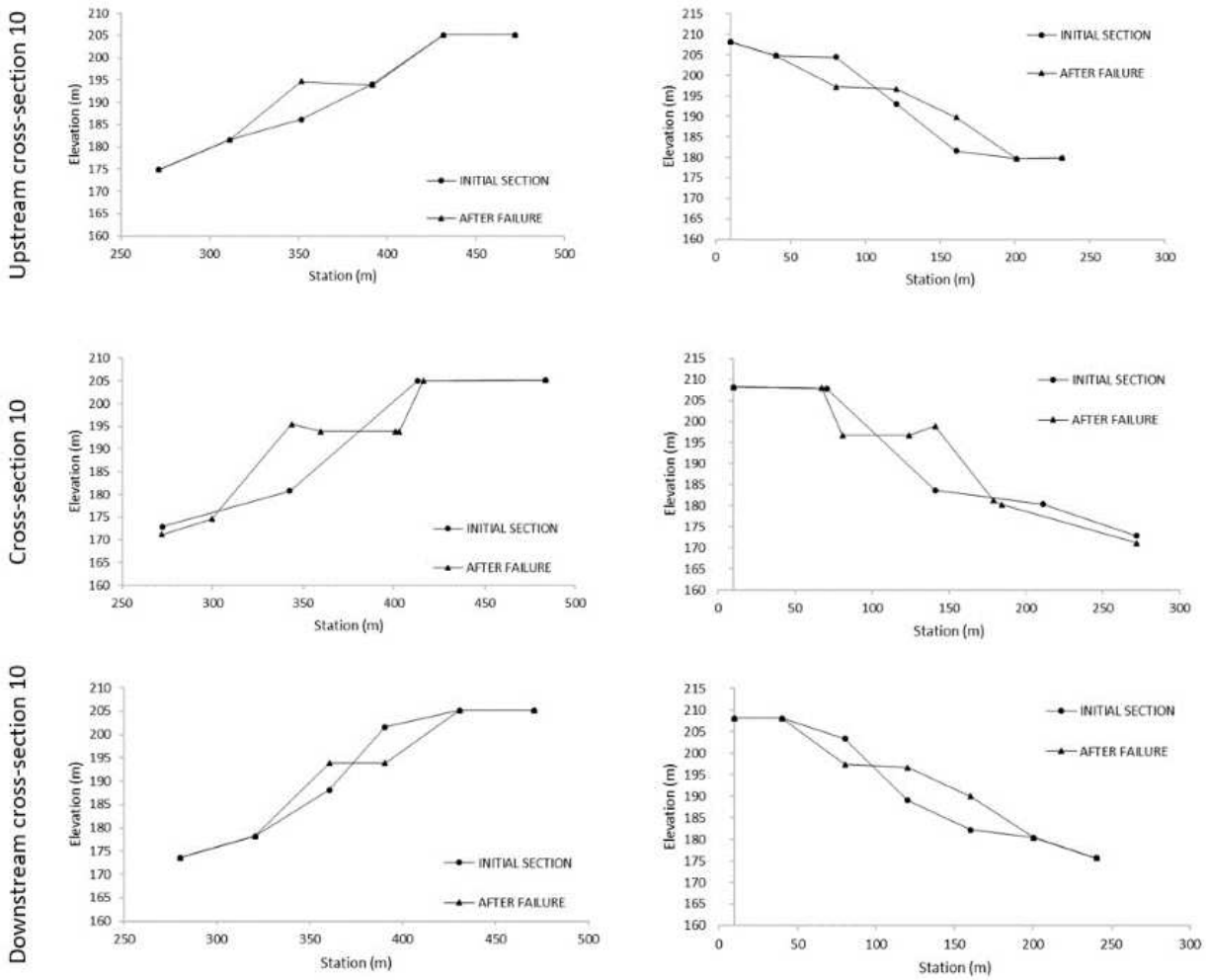

703

704 **Fig. 6.** The left and right bank profiles for cross-sections upstream and downstream cross-section 10.

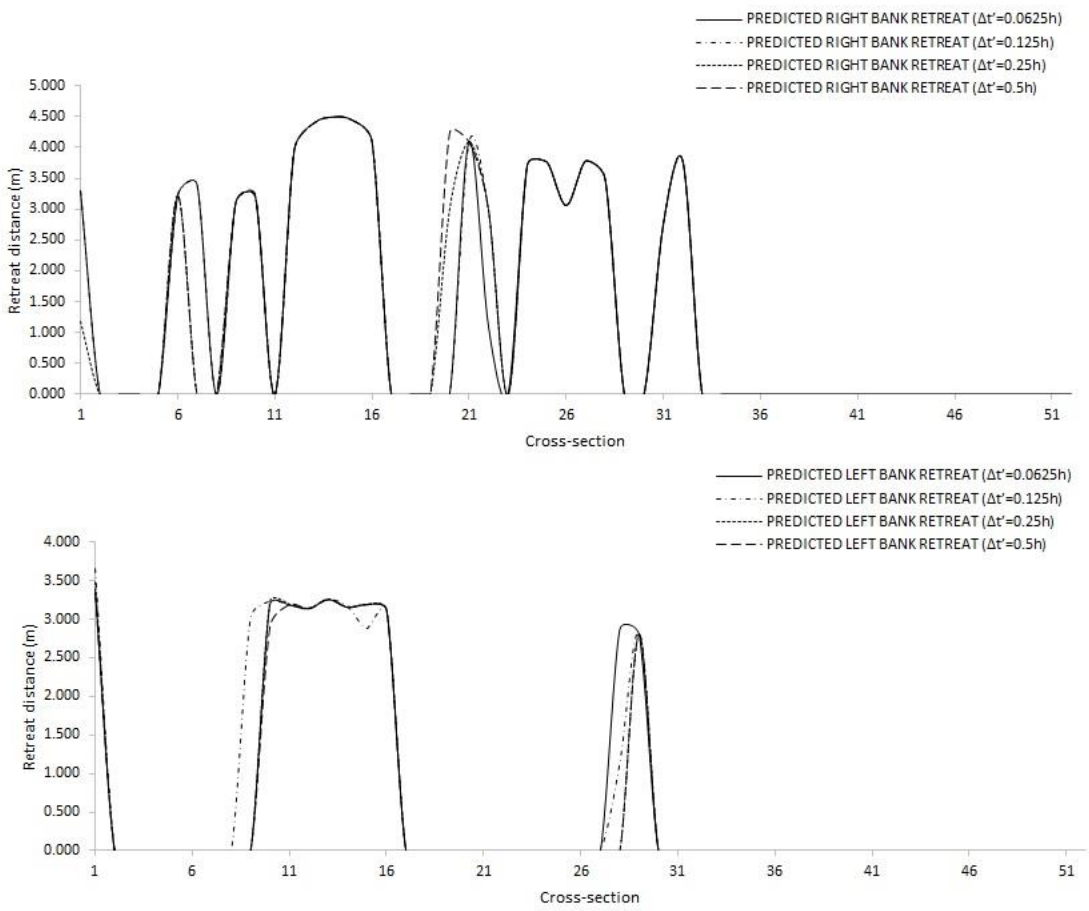

705

706 **Fig. 17.** The net bank retreat sensitivity to the BISHOP time step for the right and the left riverbanks.

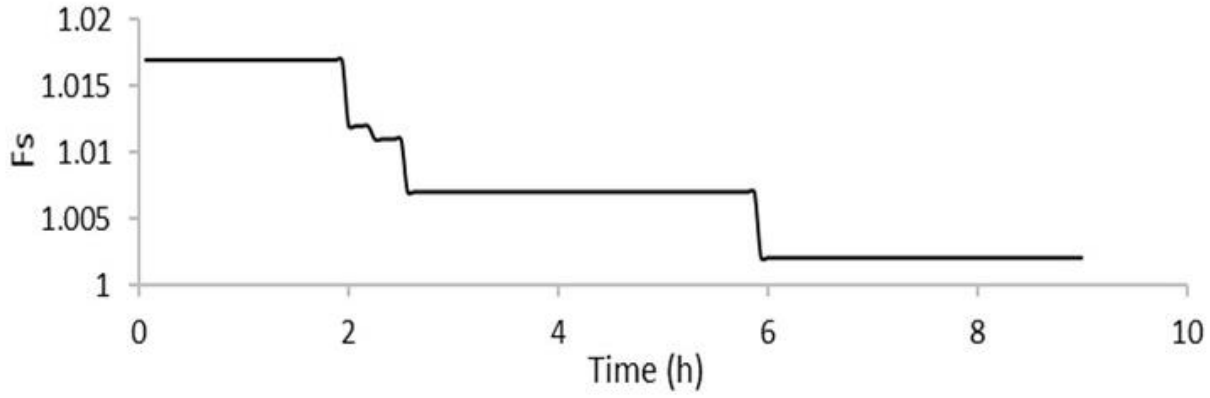

707

708 **Fig. 18.** The evolution of the factor of safety of the right bank at cross-section 9.

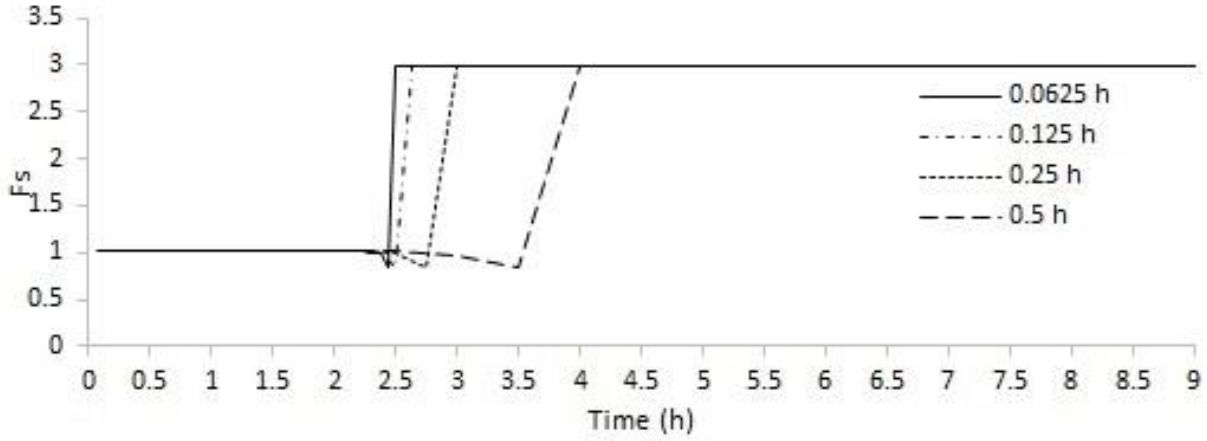

Fig. 19. The evolution of the factor of safety of the right bank at cross-section 10 considering four different geotechnical time steps.

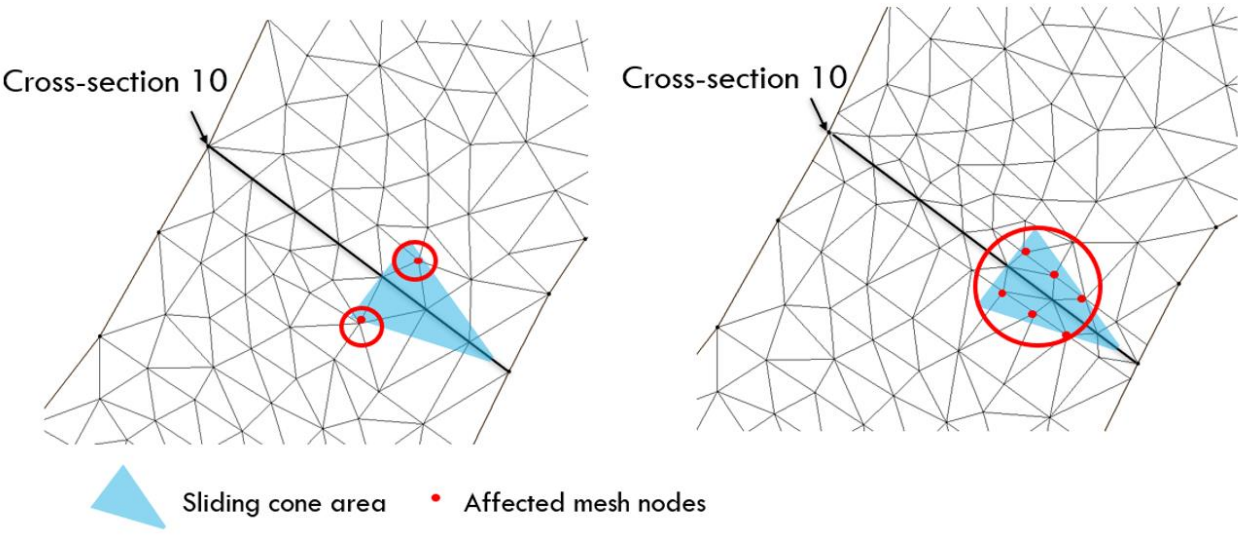

Fig. 20. Sliding cone area and affected mesh nodes before and after refining the mesh for cross section 10.